

1 **Miniature paleo-speleothems from the earliest Ediacaran (635**
2 **Ma) Doushantuo cap dolostone in South China and their implications**
3 **for terrestrial ecosystems**

4 Tian Gan^{1,2,3,4}, Guanghong Zhou^{5,6*}, Taiyi Luo^{1*}, Ke Pang³, Mingzhong Zhou⁷,
5 Weijun Luo⁸, Shijie Wang⁸, Shuhai Xiao^{2*}

6 ¹ *State Key Laboratory of Ore Deposit Geochemistry, Institute of Geochemistry, Chinese Academy*
7 *of Sciences, Guiyang 550081, China*

8 ² *Department of Geosciences, Virginia Tech, Blacksburg, VA 24061, USA*

9 ³ *State Key Laboratory of Palaeobiology and Stratigraphy, Nanjing Institute of Geology and*
10 *Palaeontology and Center for Excellence in Life and Paleoenvironment, Chinese Academy of Sciences,*
11 *Nanjing, 210008*

12 ⁴ *University of Chinese Academy of Sciences, Beijing 101408, China*

13 ⁵ *School of Geography and Resources, Guizhou Education University, Guiyang 550018, China*

14 ⁶ *Guizhou Provincial Key Laboratory of Geographic State Monitoring of Watershed, Guizhou*
15 *Education University, Guiyang 550018, China*

16 ⁷ *School of Geographical and Environmental Sciences, Guizhou Normal University, Guiyang*
17 *550001, China*

18 ⁸ *State Key Laboratory of Environmental Geochemistry, Institute of Geochemistry, Chinese*
19 *Academy of Sciences, Guiyang 550081, China*

20 *E-mail address: zhouguanghong@gznc.edu.cn; luotaiyi@vip.gyig.ac.cn; xiao@vt.edu.

21 **Abstract**

22 A rapid transition from the snowball Earth to the ‘greening’ Earth in the early
23 Ediacaran, triggered by enhanced terrestrial weathering and then by elevated primary
24 productivity, has been speculated by isotope researches³. However, direct geological
25 evidence of continental weathering in the early Ediacaran is still lacking. This study
26 examines paleo-speleothems related to the karstic dissolution surface at the upmost cap
27 dolostone of the early Ediacaran Doushantuo Formation (635 Ma). Observation of

28 sheet-crack thin-sections from platform to slope facies in South China suggests that
29 plentiful speleothem-like structures in chalcedony should be interpreted as low-
30 temperature silicified calcareous paleo-speleothems. Furthermore, isopachous dolomite,
31 speleothems, chalcedony, and quartz should have filled sheet-cracks during the uplift,
32 karstification, and subsequently hydrothermal processes before the secondary
33 transgression. Thus, these widely distributed paleo-speleothems, which are direct
34 geological evidence for the 'greening' Earth in the early Ediacaran, might represent an
35 initial formation of the soil-ecosystem after the barren snowball Earth.

36 **1. Introduction**

37 Paleo-climate evolution in the Neoproterozoic (1,000-542 Ma), the most notable
38 of which was the abrupt climate transition in the aftermath of the Marinoan deglaciation
39 (~635 Ma ⁴) recorded in the 3-5 m cap dolostones and its idiosyncratic sedimentary
40 structure, was the prelude to the Cambrian explosion. Isotopic studies ¹⁻³ have described
41 a rapid evolution from a snowball Earth to a 'greening' Earth, which could greatly
42 enhance groundwater influx of photosynthetic carbon from phytomass and promote the
43 'clay mineral factory', and then subsequently increase the atmosphere's O₂ content ⁵ and
44 trigger the expansion of multicellular life. This rapid evolution centered on a drastic
45 change of the continental weathering mode which elevated the bio-available P flux and
46 promoted the marine primary productivity. Therefore, geological records of
47 contemporaneous continental weathering are important clues to understanding the
48 evolution of life in the Neoproterozoic and to illuminating the Cambrian explosion.

49 Karstification is the most important continental weathering process in carbonate
50 distribution zones, of which the environment change could be record by speleothems
51 (stalagmites, stalactites, flowstones etc.). Studies of modern karst caves suggest that
52 speleothem deposition is mostly controlled by evolution of CO₂ contents in drip-water,
53 which originate from precipitation (atmospheric CO₂) and supersaturation in soil zone
54 (CO₂ from bio-respiration and organic decomposition) and then degassing in caves ⁶⁻⁸.

55 Thus paleo-speleothems in paleo-karst, such as dripstone ⁹, micro-stalactite ^{10,11} and
56 stromatolitic laminae coatings ¹², are significant evidence for subaerial exposure and
57 paleo-pedogenesis. The widespread discontinuous karstic surface at the top of cap
58 dolostones (635 Ma) in Africa, Canada and China has disclosed a global karstic
59 dissolution event ¹³ caused by uplifting of continental shelf responding to deglacial
60 isostatic rebound ¹⁴. Hence, more detailed geological evidence such as paleo-
61 speleothems are expected to be preserved in fissures, voids and sheet-cracks related to
62 the karstic dissolution event ¹³.

63 In this paper, we report a series of miniature but delicate paleo-speleothems
64 (including stalagmites, stalactites and coatings) preserved in the sheet-crack of
65 Marinoan cap dolostone (~635 Ma) in South China. These paleo-speleothems further
66 confirm the possibility of a broad and transient continental uplift with exposure and
67 continental weathering due to the deglacial isostatic rebound.

68 **2. Geological setting and observations**

69 The Doushantuo Formation of basin, slope and platform facies is widely deposited
70 on the Yangtze Block of South China (see Fig.1 in ref. ¹³), and is underlain by Marinoan
71 deglacial tillite unit. This shows a transition from purple diamictite (<100 m) in platform
72 facies to grey diamictite (>1000 m) in basin facies. The 3-5 m cap dolostone in basal
73 Doushantuo Formation from platform to slope facies is significant with disrupted
74 massive dolomicrite and unique structures (such as giant wave ripples ¹⁵, teepee-like,
75 sheet-cracks etc. ¹⁶). A broadly karstic dissolution surface, caused by uplift by isostatic
76 rebound, has been confirmed by geological observation in South China. The total
77 duration (<1.0 Ma) from deposition to exposure and dissolution of the cap dolostone
78 has been constrained by high-precision U-Pb zircon age of 634.57 ± 0.88 Ma at the
79 topmost of Nantuo diamictite ⁴ and 635.23 ± 0.57 Ma at the topmost of cap dolostone
80 ^{17,18}, respectively. Remarkably, sheet-cracks have a uniform mineral paragenetic
81 sequence across the entire Yangtze Block: they start with isopachous dolomites

82 (sometimes with minor barite), followed by siliceous minerals (chalcedony and quartz),
83 and ending with later stage calcite and barite ¹⁹.

84 Miniature but perfect stalactites and stalagmites, which are the most typical
85 calcareous speleothems (gravitational dripping water forms) (Fig.1, Fig.2), have been
86 gradually disclosed in chalcedony cements from thick (more than 2-3 cm) sheet-cracks
87 of cap dolostones and distributing from slope (Wenghui and Daping) to platform facies
88 (Xiaofenghe and Beidoushan) sections on the Yangtze Block. Based on this discovery,
89 flat and thinner laminae, partly with botryoidal structures, that extensively encrust the
90 ceiling and floor of the sheet-cracks or breccias (Fig.3), have been interpreted here as
91 coatings (non-gravitational water-film forms).

92 **2.1 stalactite**

93 Many stalactites, hanging downwards from the ceiling of sheet-cracks and
94 exhibiting as single one or conjoined by multi-stalactites, have been found in the
95 Beidoushan and Wenghui sections (Fig. 1, 2a, 2e and 2d). The most common individual
96 stalactites are elongated columns, ranging from less than 0.4 cm to about 1.0 cm in
97 diameter, and from less than 1 cm to more than 3 cm in length.

98 Three growth stages could be identified by laminae rhythm in two vertical profiles
99 of stalactites from the Beidoushan section (Fig.1). The first is the straight soda-straw
100 with a central channel. The channel is about 100 μm in diameter and 1-2 cm in length
101 and is lined by brown organisms and filled with cryptocrystalline chalcedony. The wall
102 of the soda-straw is comprised of fibrous chalcedony with about 400-500 μm thickness
103 and it is also coated by brown organisms. The second stage is distinguished by density
104 rippling lamina couplets in flank and botryoid structures in the tip, which reflect stable
105 and slow feeding. The final stage is composed of relative broader lamina couplets which
106 reflect continuous and affluent feeding.

107 The cross-profiles of stalactites are distinguished by multilayer concentric
108 circularity structures with alternations from dark to light. The significant difference,
109 however, is the soda-straw structure, which is generally present in stalactites but

110 absolutely absent in stalagmites. The three growth stages described above can be clearly
111 observed in the cross-profiles of stalactites from the Beidoushan section. In the
112 Wenghui section, however, only two growth stages are displayed in the cross-profiles
113 of stalactites (Fig.2a, 2e and 2d) and in the vertical-profile of stalagmites. These
114 differences suggest that the two sections have different paleo-environments.

115 **2.2 stalagmite**

116 Some stalagmites, which grow upwards from the floor of the sheet-crack, were
117 discovered in Wenghui, Xiaofenghe and Beidoushan sections. They are mainly
118 composed of translucent chalcedony, which makes them obviously distinguished from
119 the surrounding white crystalline quartz in hand-specimens of the Wenghui and
120 Beidoushan sections (Fig.2b, 2d and 2f). Most of them are cylindric in shape, slightly
121 wider in the root and narrower in the tip, with length concentrated around 1-3.5 cm and
122 diameters of about 0.5-1.3 cm. This thin diameter style, classified as "Minimum-
123 diameter" stalagmite²⁰, is coincident with the short drip fall height²¹ in the sheet-cracks.

124 A perfect vertical profile of stalagmite from the Wenghui section shows a clear
125 transition of growth style (Fig.2b) under a reflecting light microscope, while, such a
126 transition is relatively blurred under transmitted light. The early growth style is
127 distinguished by a stacked botryoid structure, which could be observed in the bottom
128 part of modern stalagmites²²⁻²⁵ (Fig.2b) and which represent turbulence of the dripping
129 water at the beginning of stalagmite deposition or indigent feeding and slow
130 precipitation²⁶. The later growth is significant with continuous and smooth rhythmical
131 laminae couplets by a dark and a light lamina, which is similar to modern calcareous
132 stalagmites^{25,27,28} and which represent affluent feeding and stable precipitation^{22,29-31}.
133 The rhythmical laminae are about 350 μm thick and contain about 20-30 lamina
134 couplets.

135 There is one complete stalagmite and three complete stalactite cross-profiles in the
136 same slide, the latter of which are characterized by a central channel texture (Fig.2d).
137 There are two growth stages. The first of these is typical of unity cryptocrystalline

138 chalcedony and the latter of them is features concentric fibrous chalcedony laminae,
139 corresponding to the two-growth style in the vertical profile as mentioned above
140 (Fig.2b). There are about 20-30 laminae couplets within the 2100 μm thick outer zone
141 and this is rich in organics as seen by the obvious increase in fluorescence (Fig.2c, 2e
142 and 2f) when compared to the inner zone. Significantly, residue calcite core and laminae
143 have been observed in one stalagmite cross-profile from the Xiaofenghe section
144 (Fig.3h).

145 **2.3 coatings**

146 In almost all of the cap dolostone sections in South China, the wall (mainly
147 composed of ceiling and floor) of the sheet-cracks and the breccias in them are
148 extensively covered with less than 0.1 cm to 1 cm thick chalcedony coatings, which
149 tend to have fairly continuous layers, and are characterized by visible rippled growth
150 morphology and stacked layering (Fig. 3). Remarkably, partly silicified calcite coatings,
151 which could be distinguished under reflected light and scanning electron microscope
152 (SEM) (Fig.3e and 3f), was preserved in the Daping section. The coatings may be
153 botryoidal (Fig. 3b), or even spiral (looks like vermiform helictites) (Fig.3c and 3d),
154 but in most cases they are smoothly curving along the wall of the sheet-crack and the
155 breccias with stable thickness (Fig. 3a). On the whole, the coatings comprise of 15-30
156 lamina couplets, which are much more obvious in ultraviolet fluorescent (Fig.2c and
157 3g), with single couplet thickness ranging from 20 μm to 60 μm . These morphology
158 and laminae structure indicate that the smooth coatings periodically precipitated from
159 adhesive water-films condensed from humid caves, the botryoidal structure are
160 produced by surface tension dividing water-films into drops and the vermiform
161 helictites produced by the addition of drip water to already present water-films.

162 **3. Discussion**

163 Protogenetic siliceous speleothems are commonly developed in caves or lava
164 tunnels overlain by silicate rocks (such as quartzites, sandstones, granites etc.)³².

165 Although platform-wide black shale overlaid on the cap dolostone ³³ seems to be a
166 potential silica source, lack of karstic surface and weathering dissolution textures in the
167 black shale suggests that the sheet-crack speleothems were not protogenetic siliceous
168 speleothems and were constrained before the deposition of the black shale. Indeed, the
169 sheet-crack speleothems are confined below the widespread paleo-karstic surface the
170 age of which has been previously determined by two ash beds with zircon U-Pb age of
171 634.57 ± 0.88 Ma and 635.23 ± 0.57 Ma ^{17,18} respectively. Additionally, the coatings in
172 the Daping section are mostly consisted of calcareous laminae (Fig. 3e and 3f) and the
173 silicified stalactites in Xiaofenghe section still retain a few calcareous laminae (Fig. 3h).
174 Therefore, the sheet-crack speleothems deposited at ca. 635Ma were originally
175 calcareous speleothems, which is akin to modern silicification-preserved speleothems
176 formed by low-temperature metasomatism of primary calcareous speleothems ^{34,35}.

177 Three successive events associated with the Marinoan cap dolostone in South
178 China have been summarized as such ¹³: (1) the first postglacial transgression and
179 deposition of the cap dolostone; (2) isostatic rebound, uplift and karstification of the
180 cap dolostone; and (3) the second postglacial transgression, multiphase cave fillings
181 and post-cap deposition. Multiple mineral generations on walls of sheet-cracks are
182 attributed to the beginning of the second postglacial transgression ¹³ or a low-
183 temperature hydrothermal episode ^{19,36}, however, minerals corresponding to the uplift
184 and karstification event have not been depicted. No obvious dissolution phenomena by
185 later erosion have been observed on the surface of the paleo-speleothems, indicating
186 that the deposition of the paleo-speleothems has been quickly terminated by the low
187 temperature hydrothermal process. Given that the hydrothermal episode developed
188 after the beginning of the second transgression, chert lens (as siliceous tufa) should be
189 observed upon the karstic surface, nevertheless, siliceous cements and veins have been
190 strictly confined beneath the karstic surface. Thus we interpret the deposition and
191 hydrothermal silicification of the sheet-crack calcareous speleothems as successive
192 processes during exposure and karstification.

193 Modern karst studies indicate that necessary condition for karstic dissolution is the
194 soil-ecosystem (soil, plant, microbial, etc.), which afford organic matter and plentiful
195 CO₂^{37,38} in the water of an epikarst zone and hence the relative speleothems could
196 partly record the overlying ecosystem information. Karst dissolution in some high-
197 altitude and cold-climate regions occurs in the absence of soil⁷, however, and so
198 obviously a temperature gradient caused by a huge altitude drop is needed to form
199 speleothems in these conditions. Paleo-karsts are defined as karsts developed largely or
200 entirely during past geological periods³⁹. Freytet (2002) refers to karsts or vugs that
201 are centimeters to decimeters as microkarsts¹¹, and these are an important evidence of
202 ancient subaerial exposure and paleosols formation^{9,11,40}. Like pseudomicrokarsts¹¹,
203 we define the microkarsts developed in past geological periods as paleomicrokarsts, in
204 which the speleothems are defined as paleomicrospeleothems. The Precambrian
205 palaeosols are habitats for early terrestrial life. The paleomicrospeleothems in the
206 corresponding carbonate strata are important geological evidence that record the early
207 biological evolution of the Earth. Paleomicrospeleothems (fibrous flowstone lining
208 grike system) found in the Mesoproterozoic in Canada⁴¹ and U.S.A³⁵ and the exquisite
209 paleomicrospeleothems (icicle-like pendants, hemispherical protrusions and ground-up
210 columns) reported in the Dengying Formation⁴² may represent contemporaneous
211 pedogenesis processes. In the early Ediacaran, although recovery of ocean-ecosystem
212 from the brutal snowball Earth had been confirmed by vase-shaped fossils in tillite, the
213 geological evidence for terrestrial-ecosystem revival are still expected yet. Here, the
214 silicified paleomicrospeleothems preserved in the 3-5 m cap dolostone suggest that the
215 soil-ecosystem had been broadly established in South China just after uplifting and
216 exposing of the cap dolostone.

217 **4. Summary and Implication**

218 This paper reports the widely distributed miniature silicified paleospeleothems in
219 sheet-cracks in Marinoan cap dolostone from South China, which depict specific karstic

220 process of the cap dolostone during uplifting and exposure caused by isostatic rebound.
221 These are 1) miniature speleothem growth during karstification; 2) speleothem
222 termination and silicification by low-temperature fluid before the second transgression.
223 These paleo-speleothems have recorded the rapid recovery of the soil-ecosystem after
224 a snowball Earth during cap dolostone rebound and karstic dissolution, which is key
225 geological evidence for the 'green' Earth model.

226 The karstic dissolution surface may have been widely distributed on a global scale
227 at early Ediacaran, implying that the coincident silicified calcareous paleo-speleothems
228 are also global distributed. The silicification preservation process has destroyed some
229 original geochemical information such as carbon/oxygen isotopes, but the plentiful
230 organic-rich laminae are preserved. Thus, the bio-markers in these organic-rich laminae
231 are expected to further document the evolution of soil-ecosystem.

232 **Acknowledgements**

233 This research was supported by the National Nature Science Fund of China
234 (41802027, 41873058), Natural Science and Technology Fund of Guizhou Province,
235 China [JZ(2015)2009], and the incentive subsidy funds from the Guizhou Education
236 University in 2019 for projects of the Ministry of Science and Technology and the
237 National Natural Science Fund of China: Study on paleo-karst structure preserved in
238 cap dolostone of Doushantuo Formation in South China. T.G. acknowledges financial
239 support from China Scholarship Council. We thank Chuanming Zhou for helpful
240 discussions and Joshua Musir for English correction.

241 **Author Contributions**

242 T.L., G.Z., and T.G. designed the research. T.L., G.Z., and T.G. collected the
243 samples. G.Z and T.G. conducted experiments. G.Z., T.L., S.X., and T.G. developed the
244 interpretation and prepared the manuscript with contributions from K.P, M.Z, W.L and
245 S.W.

246 **Methods**

247 Three sheet-crack samples (14XFH-1, 14XFH-3 and 14XFH-5) from Xiaofenghe
248 section (N30°48'54", E111°03'20"), Hubei Provinces, three sheet-crack samples
249 (14DPc1-1, 14DPc1-2 and 14DPc1-3) from Daping section (N28°59'01", E110°27'42"),
250 Hunan Provinces, four sheet-crack samples (16WH-1, 16WH-2, 16WH-3 and 16WH-
251 4) from Wenghui section (N27°49'55", E109°01'32") , Guizhou Provinces and four
252 samples (18BDS-2, 18BDS-4, 18BDS-7 and 18BDS-9) from Beidoushan section
253 (N27°01'40", E107°23'22"), Guizhou Provinces were collected from the cap dolostone
254 of the Doushantuo Formation in South China. Petrographic slices (100 µm and 200 µm
255 in thickness) and polished slabs of the sheet-crack samples were cut both perpendicular
256 and horizontal to bedding plane and investigated under transmitted light microscopy
257 (TLM), reflected light microscopy (RLM) and fluorescent light microscopy (FLM).

258

259 **Reference**

- 260 1 Kennedy, M., Droser, M., Mayer, L. M., Pevear, D. & Mrofka, D. Late Precambrian
261 oxygenation; inception of the clay mineral factory. *Science* **311**, 1446-1449 (2006).
- 262 2 Knauth, L. P. & Kennedy, M. J. The late Precambrian greening of the Earth. *Nature* **460**, 728
263 (2009).
- 264 3 Kump, L. R. Hypothesized link between Neoproterozoic greening of the land surface and the
265 establishment of an oxygen-rich atmosphere. *Proceedings of the National Academy of Sciences* **111**,
266 14062-14065 (2014).
- 267 4 Condon, D. *et al.* U-Pb ages from the neoproterozoic Doushantuo Formation, China. *Science*
268 **308**, 95-98, doi:10.1126/science.1107765 (2005).
- 269 5 Zhou, C., Yuan, X., Xiao, S., Chen, Z. & Hua, H. Ediacaran integrative stratigraphy and
270 timescale of China. *Science China Earth Sciences* **62**, 7-24, doi:10.1007/s11430-017-9216-2 (2019).
- 271 6 Baker, A., Barnes, W. L. & Smart, P. L. Speleothem luminescence intensity and spectral
272 characteristics: Signal calibration and a record of palaeovegetation change. *Chemical Geology* **130**, 65-
273 76, doi:https://doi.org/10.1016/0009-2541(96)00003-4 (1996).
- 274 7 Frisia, S. & Borsato, A. in *Developments in Sedimentology* Vol. 61 (eds A. M. Alonso-Zarza
275 & L. H. Tanner) 269-318 (Elsevier, 2010).
- 276 8 Dorr, H. & Munnich, K. O. Annual Variations of the 14C Content of Soil CO₂. *Radiocarbon*
277 **28**, 338-345 (1986).
- 278 9 Amodio, S., Barattolo, F. & Riding, R. Early Cretaceous dendritic shrub-like fabric in

- 279 karstified peritidal carbonates from southern Italy. *Sedimentary Geology* **373**, 134-146,
280 doi:10.1016/j.sedgeo.2018.06.001 (2018).
- 281 10 Qing, H. & Nimegeers, A. R. Lithofacies and depositional history of Midale carbonate-
282 evaporite cycles in a Mississippian ramp setting, Steelman-Bienfait area, southeastern Saskatchewan,
283 Canada. *Bulletin of Canadian Petroleum Geology* **56**, 209-234, doi:10.2113/gscpgbull.56.3.209 (2008).
- 284 11 Freytet, P. & Verrecchia, E. P. Lacustrine and palustrine carbonate petrography: an overview.
285 *Journal of Paleolimnology* **27**, 221-237, doi:10.1023/a:1014263722766 (2002).
- 286 12 Alvaro, J. J. & Clausen, S. Microbial crusts as indicators of stratigraphic diastems in the
287 Cambrian Breche a Micmacca, Atlas Mountains of Morocco. *Sedimentary Geology* **185**, 255-265,
288 doi:10.1016/j.sedgeo.2005.12.025 (2006).
- 289 13 Zhou, C., Bao, H., Peng, Y. & Yuan, X. Timing the deposition of ¹⁷O-depleted barite at the
290 aftermath of Nantuo glacial meltdown in South China. *Geology* **38**, 903-906 (2010).
- 291 14 Hoffman, P. F. & Macdonald, F. A. Sheet-crack cements and early regression in Marinoan
292 (635 Ma) cap dolostones: Regional benchmarks of vanishing ice-sheets? *Earth and Planetary Science*
293 *Letters* **300**, 374-384, doi:10.1016/j.epsl.2010.10.027 (2010).
- 294 15 Allen, P. A. & Hoffman, P. F. Extreme winds and waves in the aftermath of a Neoproterozoic
295 glaciation. *Nature* **433**, 123, doi:10.1038/nature03176 (2005).
- 296 16 Jiang, G., Kennedy, M. J., Christie-Blick, N., Wu, H. & Zhang, S. Stratigraphy, sedimentary
297 structures, and textures of the late Neoproterozoic Doushantuo cap carbonate in South China. *Journal of*
298 *Sedimentary Research* **76**, 978-995 (2006).
- 299 17 Zhou, C., Lang, X., Huyskens, M. H., Yin, Q.-Z. & Xiao, S. Calibrating the terminations of
300 Cryogenian global glaciations. *Geology* **47**, 251-254, doi:10.1130/g45719.1 (2019).
- 301 18 Condon, D. *et al.* U-Pb Ages from the Neoproterozoic Doushantuo Formation, China. *Science*
302 **308**, 95-98 (2005).
- 303 19 Zhou, G., Luo, T., Zhou, M., Xing, L. & Gan, T. A ubiquitous hydrothermal episode recorded
304 in the sheet-crack cements of a Marinoan cap dolostone of South China: Implication for the origin of the
305 extremely C-13-depleted calcite cement. *Journal of Asian Earth Sciences* **134**, 63-71,
306 doi:10.1016/j.jseaes.2016.11.007 (2017).
- 307 20 Fairchild, I. J. & Baker, A. *Speleothem science: from process to past environments*. Vol. 3
308 (John Wiley & Sons, 2012).
- 309 21 Gams, I. Contribution to morphometrics of stalagmite. *Proceedings of the 8th International*
310 *Congress of Speleology* **8**, 276-278 (1981).
- 311 22 Tan, M. *et al.* Applications of stalagmite laminae to paleoclimate reconstructions: Comparison
312 with dendrochronology/climatology. *Quaternary Science Reviews* **25**, 2103-2117,
313 doi:https://doi.org/10.1016/j.quascirev.2006.01.034 (2006).
- 314 23 Baker, A., Smart, P. L., Edwards, R. L. & Richards, D. A. ANNUAL GROWTH BANDING
315 IN A CAVE STALAGMITE. *Nature* **364**, 518-520, doi:10.1038/364518a0 (1993).
- 316 24 Tan, L. *et al.* Quantitative temperature reconstruction based on growth rate of annually-layered
317 stalagmite: a case study from central China. *Quaternary Science Reviews* **72**, 137-145,
318 doi:10.1016/j.quascirev.2013.04.022 (2013).
- 319 25 Railsback, L. B. *et al.* The timing, two-pulsed nature, and variable climatic expression of the
320 4.2 ka event: A review and new high-resolution stalagmite data from Namibia. *Quaternary Science*

- 321 *Reviews* **186**, 78-90, doi:<https://doi.org/10.1016/j.quascirev.2018.02.015> (2018).
- 322 26 Dreybrodt, W. & Romanov, D. REGULAR STALAGMITES: THE THEORY BEHIND
323 THEIR SHAPE. *Acta Carsologica* **37**, 175-184 (2008).
- 324 27 Tan, L. *et al.* Quantitative temperature reconstruction based on growth rate of annually-layered
325 stalagmite: A case study from central China. *Quaternary Science Reviews* **72**, 137-145 (2013).
- 326 28 Baker, A., Smart, P. L., Edwards, R. L. & Richards, D. A. Annual growth banding in a cave
327 stalagmite. *Nature* **364**, 518-520 (1993).
- 328 29 Baker, A., Proctor, C. J. & Barnes, W. L. Stalagmite lamina doublets: a 1000 year record of
329 extreme winters in NW Scotland. *International Journal of Climatology* **22** (2002).
- 330 30 Wang, X. *et al.* PRELIMINARY ANALYSES BY SIMS ON TRACE COMPONENTS OF
331 STALAGMITE MICROLAYERS AND THEIR CLIMATE SIGNIFICANCE. *Quaternary Science Reviews* **19**, 59-
332 66,97-98 (1999).
- 333 31 Brook, G. A., Rafter, M. A., Railsback, L. B., Sheen, S. W. & Lundberg, J. A high-resolution
334 proxy record of rainfall and ENSO since AD 1550 from layering in stalagmites from Anjohibe Cave,
335 Madagascar. *Holocene* **9**, 695-705, doi:10.1191/095968399677907790 (1999).
- 336 32 Aubrecht, R., Brewercarias, C., Smida, B., Audy, M. & Kovacik, L. Anatomy of biologically
337 mediated opal speleothems in the World's largest sandstone cave: Cueva Charles Brewer, Chimantá
338 Plateau, Venezuela. *Sedimentary Geology* **203**, 181-195 (2008).
- 339 33 R. C., T. T. & Y, X. *Research on Sinian Strata with ore deposits in the Yangzi (Yangtze) region,*
340 *China.* (1989).
- 341 34 Wheeler, W. H. & Textoris, D. A. Triassic Limestone and Chert of Playa Origin in North
342 Carolina. *Journal of Sedimentary Research* **48**, 765-776 (1978).
- 343 35 Skotnicki, S. J. & Knauth, L. P. The Middle Proterozoic Mescal Paleokarst, Central Arizona,
344 U.S.A.: Karst Development, Silicification, and Cave Deposits. *Journal of Sedimentary Research* **77**,
345 1046-1062 (2007).
- 346 36 Cui, Y. *et al.* Germanium/silica ratio and rare earth element composition of silica-filling in
347 sheet cracks of the Doushantuo cap carbonates, South China: Constraining hydrothermal activity during
348 the Marinoan snowball Earth glaciation. *Precambrian Research*, 105407,
349 doi:<https://doi.org/10.1016/j.precamres.2019.105407> (2019).
- 350 37 Blyth, A. J. *et al.* Molecular organic matter in speleothems and its potential as an
351 environmental proxy. *Quaternary Science Reviews* **27**, 905-921 (2008).
- 352 38 Kaufmann, G. Stalagmite growth and palaeo-climate: the numerical perspective. *Earth and*
353 *Planetary Science Letters* **214**, 251-266 (2003).
- 354 39 Bosak, P., Ford, D. C., Glazek, J. & Horacek, I. (Academia, Publishing House of the
355 Czechoslovak Academy of Sciences, Prague, Czechoslovakia, 1989).
- 356 40 Semeniuk, V., Percival, I. G. & Brocx, M. Subaerial disconformities, microkarst and paleosols
357 in Ordovician limestones at Bowan Park and Cliefden Caves, New South Wales, and their geoheritage
358 significance. *Australian Journal of Earth Sciences* **66**, 891-906, doi:10.1080/08120099.2019.1577297
359 (2019).
- 360 41 Kerans, C. & Donaldson, J. A. *Proterozoic Paleokarst Profile, Dismal Lakes Group, N.W.T.,*
361 *Canada 1.* (1988).
- 362 42 Ding, Y. *et al.* Cavity-filling dolomite speleothems and submarine cements in the Ediacaran

363 Dengying microbialites, South China: Responses to high-frequency sea-level fluctuations in an
364 'aragonite-dolomite sea'. *Sedimentology*, doi:10.1111/sed.12605 (2019).

365 **Figure Legends**

366 **Figure 1 | Polished slab and micrographs of stalactite from Beidoushan**
367 **section. a**, Polished slab shows stalactites in a sheet-crack scanning by a HP ScanJet,
368 the white solid rectangle highlights a column (connective bodies of stalactite and
369 stalagmite), white dotted rectangles highlight conjunction stalactites, the yellow arrow
370 denotes a single complete stalactite with “soda straw” drip channel. **b**, Petrographic slice
371 shows transverse and vertical sections of stalactite under TLM (transmission light
372 microscope), the white and red arrows denote the vertical and transverse sections of
373 “soda straw” drip channel, respectively. **c**, Enlarged view of the stalactite vertical
374 section in **b** (rectangle) under FLM (fluorescent light microscope), the white arrow
375 denotes the vertical section of “soda straw” drip channel. **d**, Enlarged view of stalactite
376 transverse in **b** (rectangle) under FLM, red arrows denote the transverse of “soda straw”
377 drip channel.

378

379 **Figure 2 | Polished slabs and micrographs of stalagmite, stalactite and coating**
380 **from Wenghui section. a**, Polished slab showing stalagmite, stalactite and coating in a
381 sheet-crack, white dotted lines highlight the coating areas in the sheet-crack, white
382 arrows denote stalactites, yellow arrows denote stalagmites. **b**, Petrographic slice shows
383 a vertical section of stalagmite and coating under RLM, white dotted lines highlight the
384 coating areas. **c**, Enlarged view of coating vertical section shows the organic-rich
385 laminae in **b** (rectangle) under FLM. **d**, Petrographic slice shows stalagmite and
386 stalactite transverses under TLM, red arrows and yellow arrows denote a single “soda
387 straw” drip channel and the aggregation of “soda straw” drip channel, respectively. **e**,
388 Enlarged view of a stalactite vertical section in **d** (rectangle) under FLM, showing the
389 organic-rich laminae and “soda straw” drip channel. **f**, Enlarged view of a stalagmite
390 transverse section in **d** (rectangle) under FLM, showing the organic laminae but lack of

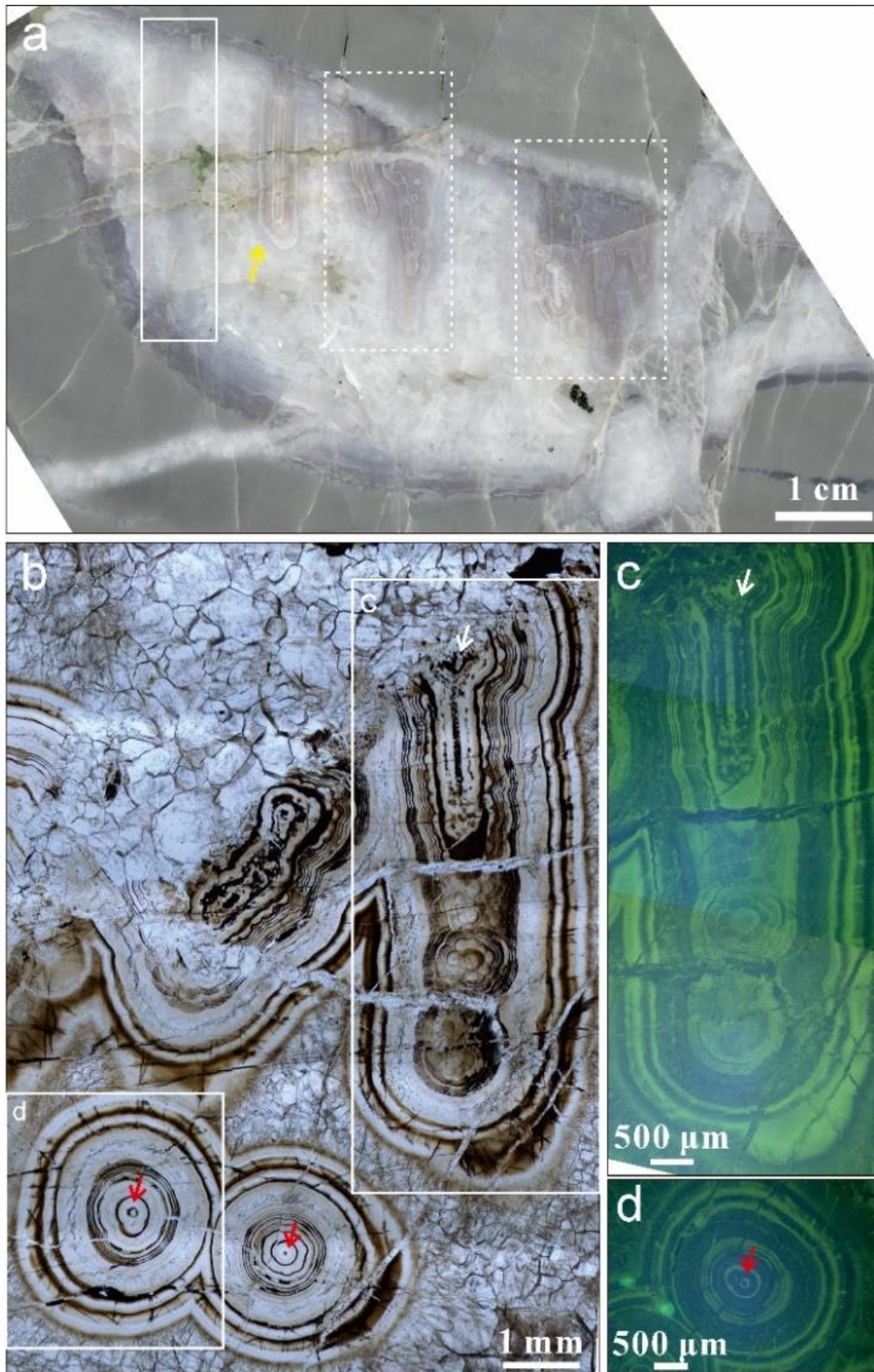
391 “soda straw” drip channel.

392

393 **Figure 3 | Polished slab, hand specimen and micrographs of coatings and a**
394 **special stalactite. a**, Polished slab shows coatings in a sheet-crack, white arrows denote
395 the coating of a dolostone breccia. **b**, Hand specimen shows a coating lining in a sheet-
396 crack, white dotted line highlights the coating boundary, black and red arrow denote
397 botryoidal and mold structure of the coating. **c**, Petrographic slice shows a coating with
398 a vermiform-like helictite under FLM. **d**, Enlarged view of the helictite in **c** (rectangle)
399 under SEM (scanning electron microscope). **e**, Petrographic slice shows a partly
400 silicified organic-rich calcareous coating under TLM. **f**, Enlarged view of the coating
401 in **e** (rectangle) under SEM, showing the silicified calcareous coating, white arrows
402 highlight the siliceous cements. **g**, Enlarged view of the coating in **e** (rectangle) under
403 FLM, showing the organic-rich laminae. **h**, Petrographic slice shows a silicified
404 stalactite under TLM, white arrows highlight the residual calcite laminae. **a, c and d**
405 from Beidoushan section, **b** from Zhangcunping section, **e-g** from Daping section, **h**
406 from Xiaofenghe section.
407

408

Fig. 1

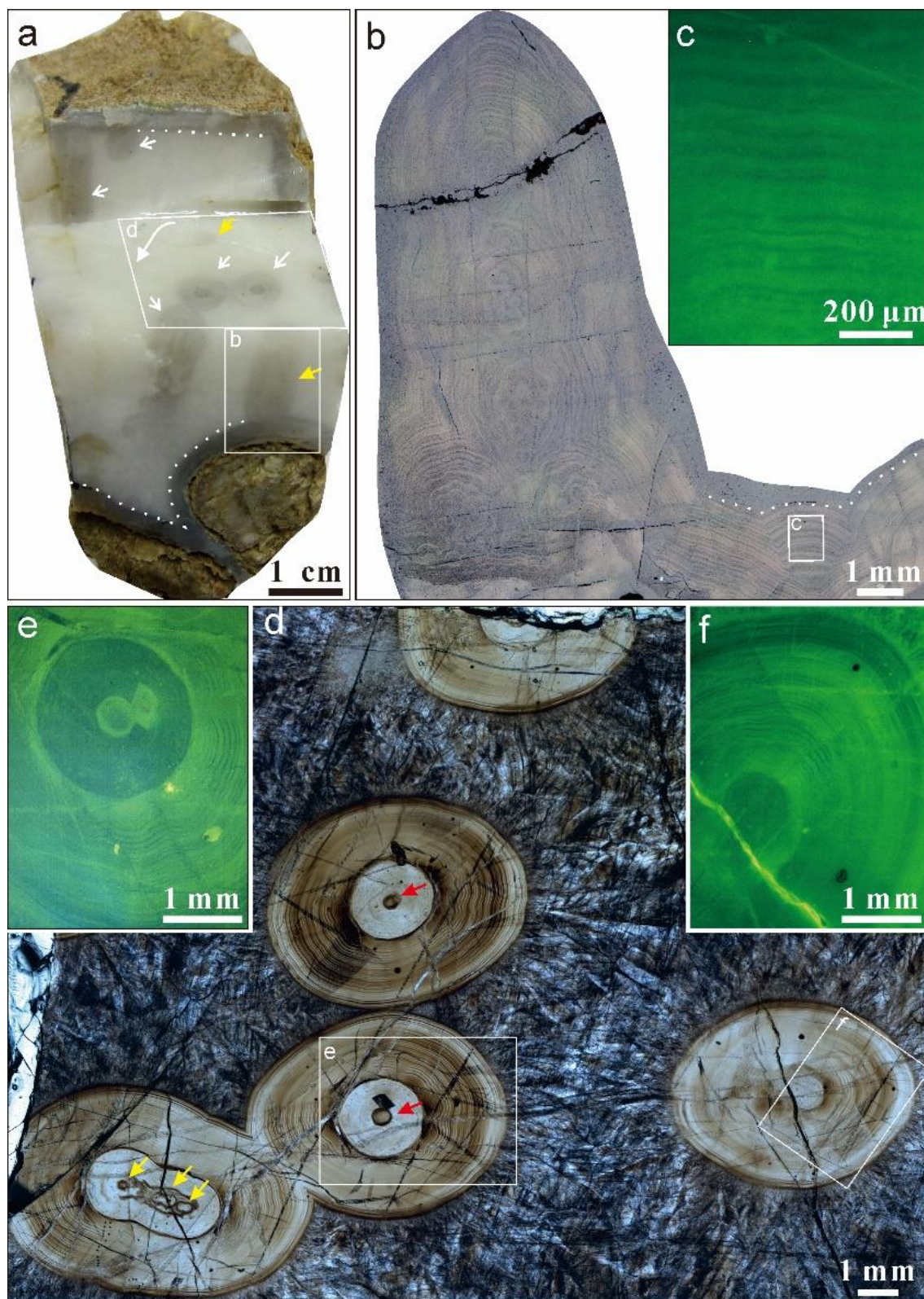


409

410

411

Fig. 2

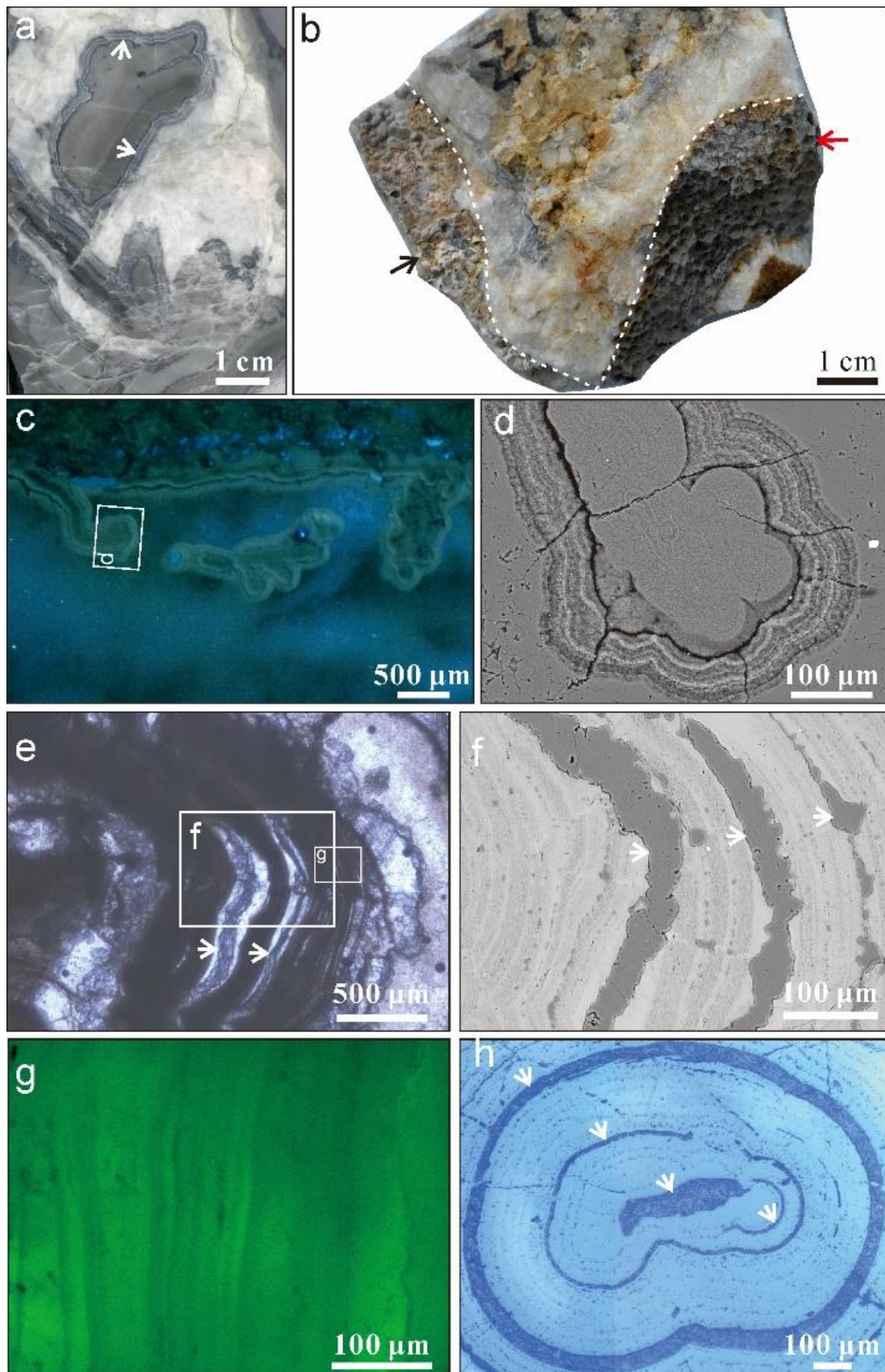


412

413

414

Fig. 3



415